Science Bulletin xxx (xxxx) xxx

Contents lists available at ScienceDirect

Science Bulletin

journal homepage: www.elsevier.com/locate/scib

Article

Mapping the electric field of high-definition transcranial electrical stimulation across the lifespan

Weiwei Ma [a,b], Feixue Wang [a,b], Yangyang Yi [a,b], Yu Huang [c], Xinying Li [a,b], Yaou Liu [d,*], Yiheng Tu [a,b,*]

[a] CAS Key Laboratory of Mental Health, Institute of Psychology, Chinese Academy of Sciences, Beijing 100101, China
[b] Department of Psychology, University of Chinese Academy of Sciences, Beijing 100049, China
[c] Research & Development, Soterix Medical Inc., Woodbridge, NJ 07095, USA
[d] Department of Radiology, Beijing Tiantan Hospital, Beijing 100070, China

ARTICLE INFO

Article history:
Received 27 March 2024
Received in revised form 23 July 2024
Accepted 24 September 2024
Available online xxxx

Keywords:
Transcranial electrical stimulation
Lifespan trajectory
Electric field
Anatomical factor
Head model

ABSTRACT

Transcranial electrical stimulation (tES) is a non-invasive technique widely used in modulating brain activity and behavior, but its effects differ across individuals and are influenced by head anatomy. In this study, we investigated how the electric field (EF) generated by high-definition tES varies across the lifespan among different demographic groups and its relationship with neural responses measured by functional magnetic resonance imaging (fMRI). We employed an MRI-guided finite element method to simulate the EF for the two most common tES montages (i.e., targeting the dorsolateral prefrontal cortex and motor cortex, respectively) in two large cohorts of white and Asian participants aged 12 to 100 years. We found that the EF intensity decreased with age, particularly in individuals under 25 years of age, and was influenced by gender and ethnicity. We identified skull thickness, scalp thickness, and epidural cerebrospinal fluid thickness, as the primary anatomical factors accounting for the inter-individual EF variability. Using a concurrent tES-fMRI approach, we observed a spatial consistency between the simulated EF and the brain activity changes induced by tES in the target region. Finally, we developed an open-source toolbox incorporating age-stratified head models to facilitate efficient EF calculations. These findings characterize and quantify the individual differences in tES-induced EF, offering a reference for implementing personalized neuromodulation strategies.

1. Introduction

Non-invasive neuromodulation via transcranial electrical stimulation (tES) has emerged as a promising tool for various scientific and therapeutic applications owing to its safety, availability and portability [1–3]. However, significant variability in outcomes across tES studies has been reported [4,5]. This variability may arise from differences in head anatomy as well as variations in neural and behavioral responses to electrical stimulation [6]. The physical influence of head anatomy on the distribution and intensity of electric currents reaching target brain regions underlies the observed variability in neural and behavioral responses. Consequently, individualized tES approaches have gained attention in recent years, as they offer the potential to optimize stimulation protocols based on individual characteristics, thereby enhancing the efficacy and reproducibility of tES interventions.

The advent of magnetic resonance imaging (MRI)-guided computational modeling with finite element analysis has enabled non-invasive investigation of the electric field (EF) distribution in individual brains [7–10]. Variations in head anatomy across age, gender and ethnic groups [11–15] lead to distinct EF distributions among demographic groups. Previous studies have devised systematic methodologies for high-resolution individualized modeling to capture fine anatomical structures and compute EF distributions based on structural MRI data [16–19]. However, existing studies utilizing MRI-guided modeling of individualized tES have mainly focused on age-related decreases in simulated EF intensity, without revealing the lifespan trajectories of intensities or the complex interaction effects of age and gender in different ethnic groups [20–29]. Furthermore, few studies have explored the application of high-definition (HD) tES, which uses multiple small electrodes, known as "high-definition" electrodes, to achieve

* Corresponding authors.
E-mail addresses: yaouliu80@163.com (Y. Liu), yihengtu@gmail.com (Y. Tu).

https://doi.org/10.1016/j.scib.2024.10.001

Please cite this article as: W. Ma, F. Wang, Y. Yi et al., Mapping the electric field of high-definition transcranial electrical stimulation across the lifespan, Science Bulletin, https://doi.org/10.1016/j.scib.2024.10.001

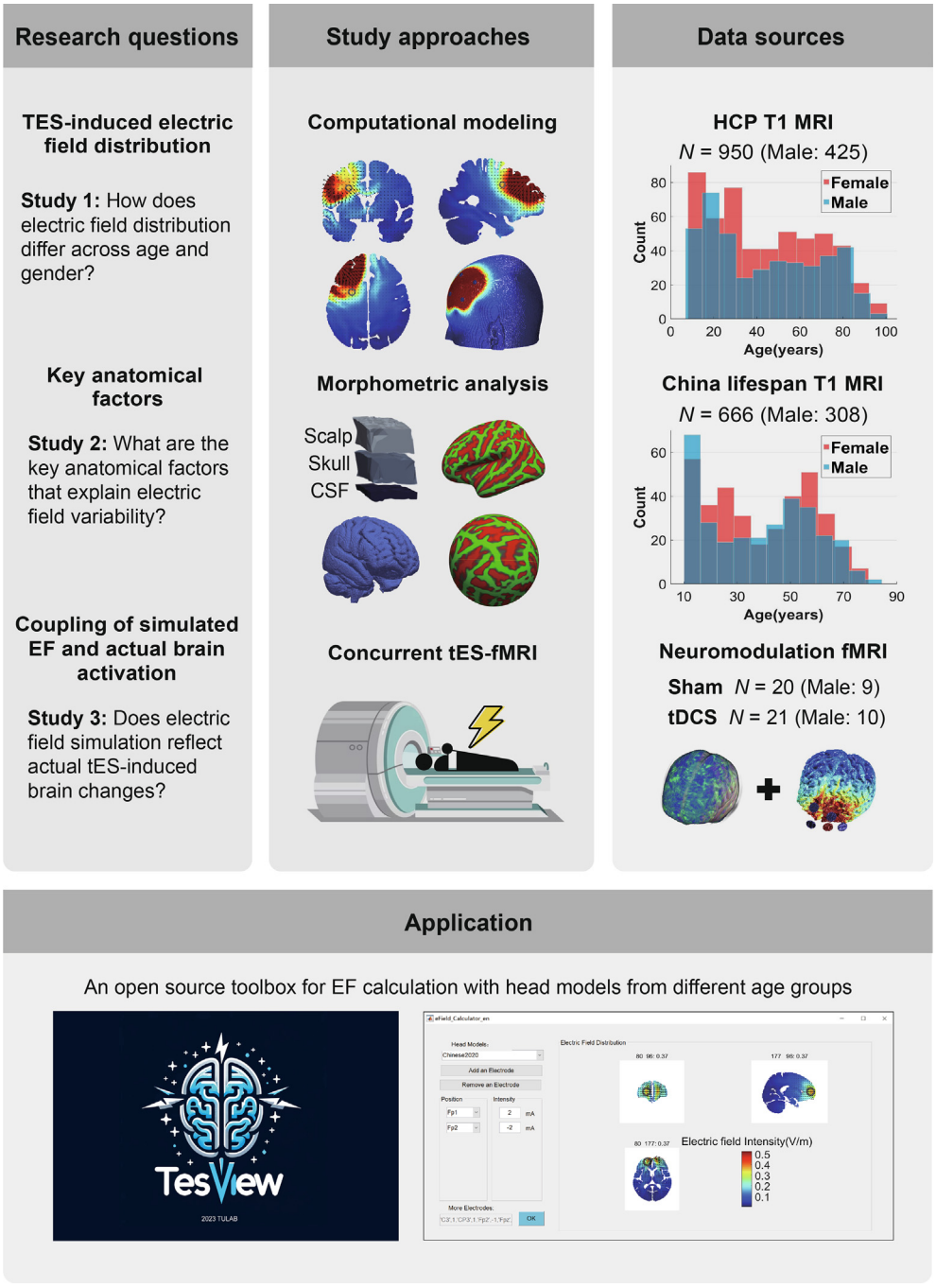

Fig. 1. Study overview with three main research questions, approaches, data sources, and a practical application of the study. The study employed a combination of analytical approaches, including computational modeling and morphometric analysis, to investigate inter-subject variability in tES-induced electric fields and identify the underlying anatomical factors based on large-scale T1 MRI data. Additionally, an experimental approach utilizing concurrent tES-fMRI was employed to obtain fALFF/degree centrality maps during stimulation and explore the relationship between simulated electric fields and induced brain activations. EF: electric field; tES: transcranial electrical stimulation; fALFF: fractional ALFF; fMRI: functional magnetic resonance imaging.

more focal stimulation and allow for maximizing brain stimulation intensity under fixed constraints on the scalp current [7].

Further studies have examined the precise anatomical factors underlying inter-individual variability in EF distribution. Factors such as cerebrospinal fluid (CSF) volume and skull thickness have been shown to heavily influence intensities in the target [20,24–26,30,31]. Moreover, scalp thickness, sulcal depth, the distance between the target region and the electrode, along with the morphology of brain structures such as gyri and sulci, also play critical roles in determining the resulting EF [20,25,30–35]. However, these factors have been investigated separately, and a comprehensive study that considers both EF intensities and focality with a larger sample size is warranted.

While computational flow-current models have been validated using scalp potentials [36] and *in vivo* intracranial recordings that capture electric current intensities [37–39], research on the functional state changes of the brain in response to electrical stimulation remains limited, which is believed to contribute to the variability in tES outcomes. Functional MRI (fMRI) reveals both local and large-scale brain responses to the stimulation. By delivering tES inside the MRI scanner, concurrent tES-fMRI offers a promising approach to elucidate the causal interactions between

extrinsic stimulation and brain neural responses [40–45]. This approach allows for the exploration of the association between simulated EF and actual brain activity changes induced by tES, providing valuable information for individualized tES.

In this study, leveraging computational modeling, tES-fMRI approaches, and lifespan (aged 12 to 100) T1 MRI data (n>1600) from both the US and China [46], we aimed to simulate the EF induced by HD-tES and to establish age trajectories of EF measures across gender and ethnic groups as a reference (Study 1). Additionally, we sought to identify key anatomical factors underlying individual differences in EF (Study 2), explore the association between the simulated EF and tES-induced changes in fMRI (Study 3), and ultimately provide an open-source toolbox with age-stratified head models designed for efficient EF calculations (Fig. 1).

2. Methods

To investigate the variability of tES-induced EF among individuals, we conducted three studies with multiple approaches. In Study 1 and 2, we combined computational modeling with morphometric analysis to assess EF distribution differences across age and gender (Study 1) and to identify the key anatomical factors contributing to the inter-individual variability (Study 2). The computational modeling in these studies was based on 1616 structural MRI scans from two lifespan cohorts: 950 scans of white participants [47] obtained from the Human Connectome Project cohort, and 666 scans of Asian individuals from a Chinese cohort. In Study 3, we employed concurrent tES-fMRI and focused on the association between simulated EF and actual brain activation patterns to explore potential functional implications. In all studies, we conducted individual simulations of tES-induced EF based on each participant's T1-weighted MRI using ROAST, a realistic, volumetric approach to simulate transcranial electrical stimulation [17].

2.1. Data sources

2.1.1. Human Connectome Project (HCP)

High-resolution T1-weighted structural magnetic resonance volumes of the white cohort (n=950, 425 males, aged 12–100) were gathered from the HCP Young-Adult (HCP-YA) project, WU-Minn Consortium [48] and Lifespan HCP in Development (HCP-D) and in Aging (HCP-A). To ensure a balanced sample size across age groups, only the 184 individuals with 7T scans from the HCP-YA project were included. Young children under 12 were excluded due to the rarity of tES applications in this age group, primarily for safety considerations. All retrieved data underwent minimal preprocessing and the extended FreeSurfer preprocessing procedure for cortical reconstruction [49]. High-resolution (0.7 mm isotropic) scanning in the HCP-YA project was conducted on a customized Connectome Skyra scanner with the following parameters: repetition time (TR) of 2400 ms, echo time (TE) of 2.14 ms, inversion time (TI) of 1000 ms, flip angle (FA) of 8°, and a field of view (FOV) of 224 mm×224 mm. For the HCP-D/A, scans were collected at four sites with 0.8 mm isotropic voxels using a 3T Siemens Prisma scanner. The scanning parameters at all sites were as follows: TR=2500 ms, TE=1.8/3.6/5.4/7.2 ms, TI=1000 ms, flip angle=8°, and sagittal FOV=256 mm×240 mm×166 mm. Overall, merging T1-weighted data from the HCP-YA and HCP-D/A cohorts was considered adequate for this study despite minor differences in scanning parameters [47].

2.1.2. China lifespan dataset

Lifespan T1-weighted structural MRI data for the Asian cohort were collected from two sites in China (n=666, 308 males, aged 14–84). MRI scans of Asian adolescents (under 20 years) were obtained from a twin cohort supported by Beijing Normal University. Approval was obtained from IRB of the Institute of Psychology, Chinese Academy of Sciences (No. H20037). These data were acquired at the Beijing MRI Center for Brain Research using a 3 T Siemens TrioTim with the following parameters: resolution of 1.3 3×0.5×0.5 mm, TR=2530 ms, TE=3.37 ms, TI=1100 ms, flip angle=7°, and FOV=192×216 mm. To mitigate inter-sample correlation arising from the similarities in head anatomy between identical twins, one twin from each set was excluded. Informed consent was obtained from all participants.

For Asian adults, data acquisition was conducted at Beijing Tiantan Hospital using three scanners, with parameters that allow for data harmonization. Detailed acquisition parameters are shown in Supplementary materials (Table S4 online). Ethical approval was granted by IRB of Beijing Tiantan Hospital, Capital Medical University (No. KY2021-150–01). Informed consent was obtained from all participants.

2.1.3. Neuromodulation fMRI dataset

In Study 3, 43 healthy volunteers were recruited and randomized into two groups: a transcranial direct current stimulation (tDCS) group and a sham group, following written informed consent. One participant withdrew from the tDCS group prematurely due to scanner-related discomfort, and another participant was excluded from the analysis due to excessive head motion. Consequently, the final sample comprised 41 participants, with 20 individuals in the sham group (9 males, age: 23.75±2.83 years) and 21 in the tDCS group (10 males, age: 22.81±2.71 years). None of the participants reported a history of neurological or psychiatric disorders. The study was first intended to investigate the modulation effects of tDCS on reward learning, approved by IRB of the Institute of Psychology, Chinese Academy of Sciences (No. H22006). All procedures were performed in accordance with the guidelines set forth by the IRB for the ethics and protection of human participants. All participants gave written consent.

Stimulation was delivered using a HD-tES stimulator (Soterix Medical, New York, USA). The MRI-compatible stimulation system, consisting of five carbon rubber electrodes embedded in a BrainCap (Brain Vision), along with a stimulation device including RF filters and resistors, was utilized to target the left orbitofrontal cortex (OFC). Electrodes were positioned in a 4×1 montage, with the anode over FP1, and cathodes over FPZ, AFZ, AF3, and AF7 based on the 10–10 EEG system. For the active group, tDCS was applied at 1.5 mA for 20 min, while the sham group received current only during a 30-second ramp-up/down phase at the start/end of a 20-minute sham stimulation period. Impedances were kept below 5 kΩ for both conditions. T1-weighted brain images were acquired using a 48-channel radio-frequency head coil in a 3.0T GE scanner, with imaging parameters as follows: TR=7.24 ms, TE=2.96 ms, flip angle=12°, and FOV=256×256 mm^2. Participants were instructed to keep their eyes open and remain awake during the resting-state scan session, and the resting-state fMRI data were acquired with gradient echo planar imaging: TR=2000 ms, TE=29 ms, flip angle=90°, FOV=225×225 mm^2, slice thickness=3.5 mm, number of slices=31, and number of volumes=240.

2.2. Computational modeling analysis

2.2.1. Electric field simulation

ROAST 3.0 was used to simulate EF through finite element method (FEM). In the ROAST pipeline, each T1-weighted image was resampled to a 1 mm isotropic resolution, underwent bias field correction, and was segmented using SPM12, followed by electrode placement. Subsequently, each image was fed into iso2-mesh to generate an optimized mesh based on individual head anatomy for EF computation in getGDP. In both Study 1 and 2,

two tES montages were selected for simulation, namely the dorsolateral prefrontal cortex (DLPFC) montage (central electrode at F3 and return electrodes at F1, FC3, F5, and AF3) and the motor cortex montage (central electrode at C3 and return electrodes at Cz, P3, T7, and F3). These high-definition montages, commonly used in prior tES studies, were simulated with a 2 mA current intensity and electrode discs of 4 mm radius and 1 mm thickness, parameters widely adopted in tES research. It should be noted that current intensities exceeding 2 mA can cause pain in most participants [50], and the input current intensities do not alter the pattern of EF distribution for a specific montage.

Additionally, to better elucidate the effects of morphology without introducing excessive confounding factors, all tissue conductivities were assumed isotropic and constant over the lifespan in this study. The conductivities values were defined as follows: σ (white matter)=0.126 S m^{-1}, σ (gray matter)=0.276 S m^{-1}, σ (CSF)=1.65 S m^{-1}, σ (skull)=0.01 S m^{-1}, σ (scalp)=0.465 S m^{-1}, σ (air)=2.5×10^{-14} S m^{-1}, σ (gel)=0.3 S m^{-1}, and σ (electrode) =5.9×10^{7} S m^{-1}. ROAST could produce abnormally large voltage values for a few T1-weighted scans, possibly related to data quality or incompatibilities with individual head anatomies. To ensure simulation quality, we excluded HCP outputs with the top 2% 95th percentile voltage and China dataset outputs with the top 5% 95th percentile voltage before removing outliers outside three standard deviations of the mean (95th percentile EF). More than 900 cases (927 for the DLPFC montage, 926 for the motor cortex montage) from the HCP dataset and over 600 (602 for the DLPFC montage, 601 for the motor cortex montage) from the China dataset were present in the final sample for further analysis.

To investigate the variations in tES-induced EF distribution across age and gender in both the white and the Asian cohort, simulation results were categorized into eight demographic groups (4 age groups$\times$2 gender groups). The four age groups were previously defined by neurobiological criteria [51]: adolescence (12 years$\leq$ age<20 years), young adulthood (20 years$\leq$age<40 years), middle adulthood (40 years$\leq$age<60 years), and late adulthood (age$\geq$60 years), with each stratified by gender.

2.2.2. Estimation of electric field intensity at regions of interest

Following the EF distribution calculation for each individual from MRI scans, the volumes of EF intensities were spatially normalized to the 246-region Brainnetome atlas [52] to establish a one-to-one correspondence between the volumes of different individuals. We then defined regions of interest (ROIs) as those with the largest intensity averages. We calculated the mean EF intensity across voxels in each of the 246 regions and averaged these mean intensities among individuals in each region separately for each of the eight demographic groups, considering potential variations in the most stimulated regions across age and gender groups. The brain regions were sorted by intensity average in descending order for each case.

For the DLPFC montage, the most stimulated regions were the ventral and dorsal areas of the left DLPFC; for the motor cortex montage, the most stimulated regions were the postcentral gyrus and the precentral gyrus. Consequently, the ventral and dorsal areas were defined as ROIs for the DLPFC montage, and the postcentral gyrus and the precentral gyrus were defined as ROIs for the motor cortex montage in both Study 1 and Study 2.

2.2.3. Calculating the focality measure

Surface reconstruction was performed with FreeSurfer [53,54] to derive the surface area measurements of the left hemisphere for each individual. Focality was determined by computing the surface area proportion of the gray matter region where EF intensities exceeded the 95th percentile. We first extracted the EF distribution within the gray matter regions of interest and then transformed the EF results into fsaverage space. The FreeSurfer pipeline enabled area measurement of this surface output, where higher area values indicated lower focality. To enhance the reliability of our measures, we divided the area with intensities over 95th percentile by the total surface area of the left hemisphere. This normalization approach mitigated the influence of head size variations, providing a clearer reflection of the relationship between the breadth and depth of the stimulated region.

2.2.4. Calculating the distance between the central electrode and the ROI

The distance between the central electrode and the ROIs was considered one of the underlying anatomical factors influencing EF variability. We extracted the coordinates of each electrode center in each individual's native space from the ROAST pipeline. Then the coordinates of ROI centers, defined in the standard MNI space, were converted to native space by applying the inverse affine matrix included in the segmentation outputs. With the locations of both the ROI center and the central electrode, we calculated the Euclidean distance between them for each individual.

2.3. Morphometric analysis

Apart from the central electrode-ROI distance, we selected eight additional factors concerning brain morphology from a set of anatomical features. To minimize correlations between independent variables, several features (total gray volume, total white volume, the distance between the head center and the central electrode, and so forth) were removed from the set (with variance inflation factor$\geq$4). Volumetric and surface-based measures, including brain volume, brain volume-total intracranial volume (TIV) ratio, sulcal depth, cortical thickness, and local gyrification index (LGI) [55], were acquired via the FreeSurfer reconstruction pipeline in each individual's native space. These measures were identified in each brain region using the 246-region Brainnetome atlas.

Additionally, post-processing in Paraview [56] was used to compute tissue thickness of the scalp, skull and epidural CSF in the native space. The mesh generated for each head model in ROAST was loaded into Paraview, and a box-shaped clip filter was applied to isolate a cuboid region of the head tissue containing the scalp, skull, epidural CSF and a portion of the gray and white matter beneath the central electrode. The box's position was defined by the locations of its corner points and the extrinsic rotation angles. Specifically, the longitudinal direction of the box (Fig. 4a) was determined by the line connecting the center of the central electrode and the individual's head center optimized in the ROAST. Subsequently, we calculated the unit direction vectors for the three sides of the box, with the constraint that one of the short sides was parallel to the sagittal plane of the head. Corner point coordinates and extrinsic rotation Euler angles were then derived from the unit direction vectors and the central electrode's location. The cross section of the box was a 15 mm$\times$15 mm square, selected to be small enough to ignore the curvature of the head surface yet large enough to capture the representative structure of the epidural CSF tissue. The length of the box was set empirically to 50 mm to ensure that it encompassed the complete epidural CSF tissue under the central electrode while excluding CSF within the brain ventricles. To estimate tissue thickness, we applied a threshold filter to the tissue cube of each head model, extracting the scalp, skull and epidural CSF tissues within the box separately. The volumes of all mesh elements for each tissue type were

summed to obtain the total volume of each tissue (denoted by V_{scalp}, V_{skull}, and V_{CSF}). Ignoring the surface curvature of each segmented head tissue, the tissue thickness was estimated as follows.

$$S_{tissue} = 15\,mm \times 15\,mm = 225\,mm^2 \quad (1)$$

$$t_{scalp} = V_{scalp}/S_{tissue} \quad (2)$$

$$t_{skull} = V_{skull}/S_{tissue} \quad (3)$$

$$t_{CSF} = V_{CSF}/S_{tissue} \quad (4)$$

2.4. Calculating distance measures for the electric field-actual activation coupling

To integrate the simulated EF with actual neural activations, we obtained the simulated EF for the OFC montage using ROAST and the corresponding neural responses through concurrent tDCS-fMRI in Study 3. Guided by T1-weighted images, EF simulation followed a protocol similar to that in Study 1 and Study 2. But the central electrode was positioned at Fp1 (1.5 mA) and return electrodes at Fpz (–0.375 mA), AFz (–0.375 mA), AF3 (–0.375 mA), and AF7 (–0.375 mA) to target the left OFC, with electrode discs of 9 mm radius and 1 mm thickness. The estimated electrode size was consistent with the experiment protocol.

Functional phase data were analyzed by calculating the fractional amplitude of low-frequency fluctuation (fALFF), a measure of local functional brain activity [57], and degree centrality (DC) [58] with a correlation threshold of 0.25 serving as a functional connectivity measure. To assess neural response changes, we obtained maps of these measures using fMRI data collected both before and during tDCS for each participant using DPABI (https://rfmri.org/DPABI) [59]. These maps were aligned with the 800-parcellation Schaefer atlas, which offers finer granularity than the 246-region Brainnetome atlas and enables more detailed characterization of local neural responses to tDCS at the OFC. By subtracting pre-stimulation maps from during-stimulation maps, we derived the difference maps of fALFF and DC. A mask of the OFC extracted from the Schaefer atlas was used to confine our analysis to the OFC region, reducing the effects of physiological noise from a wider range of brains and enhancing sensitivity in detecting changes.

To verify the correspondence between the average simulated EF intensity and average fALFF/DC change, we identified the site of maximum EF intensity and the site of maximum fALFF/DC change within the OFC for each individual. These sites were visualized by superimposing them on a common surface template (Fig. 5b). The Euclidean distance between them for each individual was calculated by:

$$D = \sqrt{\left(x_{EF} - x_{fALFF/DC}\right)^2 + \left(y_{EF} - y_{fALFF/DC}\right)^2 + \left(z_{EF} - z_{fALFF/DC}\right)^2} \quad (5)$$

where x_{EF}, x_{EF} and z_{EF} denote coordinates of the maximum EF intensity subregion, while $x_{fALFF/DC}$, $x_{fALFF/DC}$ and $z_{fALFF/DC}$ denote coordinates of the maximum fALFF or DC change subregion.

2.5. Statistical analysis

In examining individual differences in EF distribution across age and gender, we conducted a two-way ANOVA on EF intensity and EF focality measures. Age (4 groups) and gender (male and female) were treated as inter-subject variables for each ROI in both ethnic cohorts. Next, we assessed the correlation between EF intensity and age, using generalized additive models (GAMs) via package mgcv [60] in R to fit age trajectories. For each case (Fig. 3), EF intensity was modeled independently as a function of the intercept and two smoothers: the gender difference and thin plate regression splines for age, formulated as follows.

$$Intensity \sim gender + s(age) + s(age, by = gender) \quad (6)$$

where the gender term denotes the intercepts for the gender group; the first $s()$ term represents the overall nonlinear effect of age on intensity, while the second $s()$ term with *by* argument estimates smooth-factor interactions, allowing comparison of the age effects between the two gender groups by learning separate smooth functions for each level of the gender factor. Each of the separate smooths based on k number of weighted basis functions was centered around zero effect, indicating differences in the developing trend of age trajectories. REML method was used for numerical stability, and k was determined based on model fit. Smooth effects of the functions were visualized with fitted GAM curves and 95% confidence interval by package ggplot2 [61].

Our focus extended to identifying key anatomical factors contributing to the individual differences in EF. To this end, stepwise linear regression models, facilitated by the MASS package [62] in R, were established with 9 variables (Fig. 4a): brain volume, brain volume-TIV ratio, sulcal depth, cortical thickness, LGI, scalp thickness, skull thickness, CSF thickness and ROI-anode distance. These models were executed separately for each montage within each ethnic group, with backward elimination based on Akaike information criterion for variable selection. The size effects of anatomical factors were estimated by calculating Cohen's f^2 [63], which evaluated their contribution in explaining individual differences. Finally, we performed an independent two-tailed t-test to compare the strength of the connection between simulated EF and actual brain activations in the tDCS group with the strength in the sham group.

3. Results

3.1. Individual differences in tES-induced electric field distribution

We conducted individual simulations of the two most commonly used tES montages in Study 1, targeting the DLPFC and the motor cortex, for each participant in the lifespan cohorts and divideed participants into eight demographic groups. The regions with the highest intensity averages for each montage were defined as ROIs. For the DLPFC montage, the ROIs were the ventral and dorsal areas of the left DLPFC, while for the motor cortex montage, the ROIs were the precentral gyrus and postcentral gyrus. In both ethnic cohorts, the brain region with the largest intensity average was the ventral area for most male groups, while it was the dorsal area for most female groups, which indicated a potential gender difference in DLPFC morphology. Group-level averages of the intensity received by the ROIs are presented in the Supplementary materials (Table S1 online). Violin plots in Fig. 2 illustrate the individual differences in tES-induced EF intensity. Adolescents had the highest intensity averages among the four age groups in all ROIs for both ethnic cohorts. Females generally received higher intensities than males, and the ROIs for the motor cortex montage showed significantly higher intensities compared to the those for the DLPFC montage. Furthermore, the intensities for the motor cortex montage showed greater differences between ethnic groups, with relatively lower intensity values observed in the Asian groups compared to the white groups.

Two-way ANOVA analysis revealed a significant main effect of age (P_{age}<1 × 10^{-42} in all ROIs for both races) and a significant main

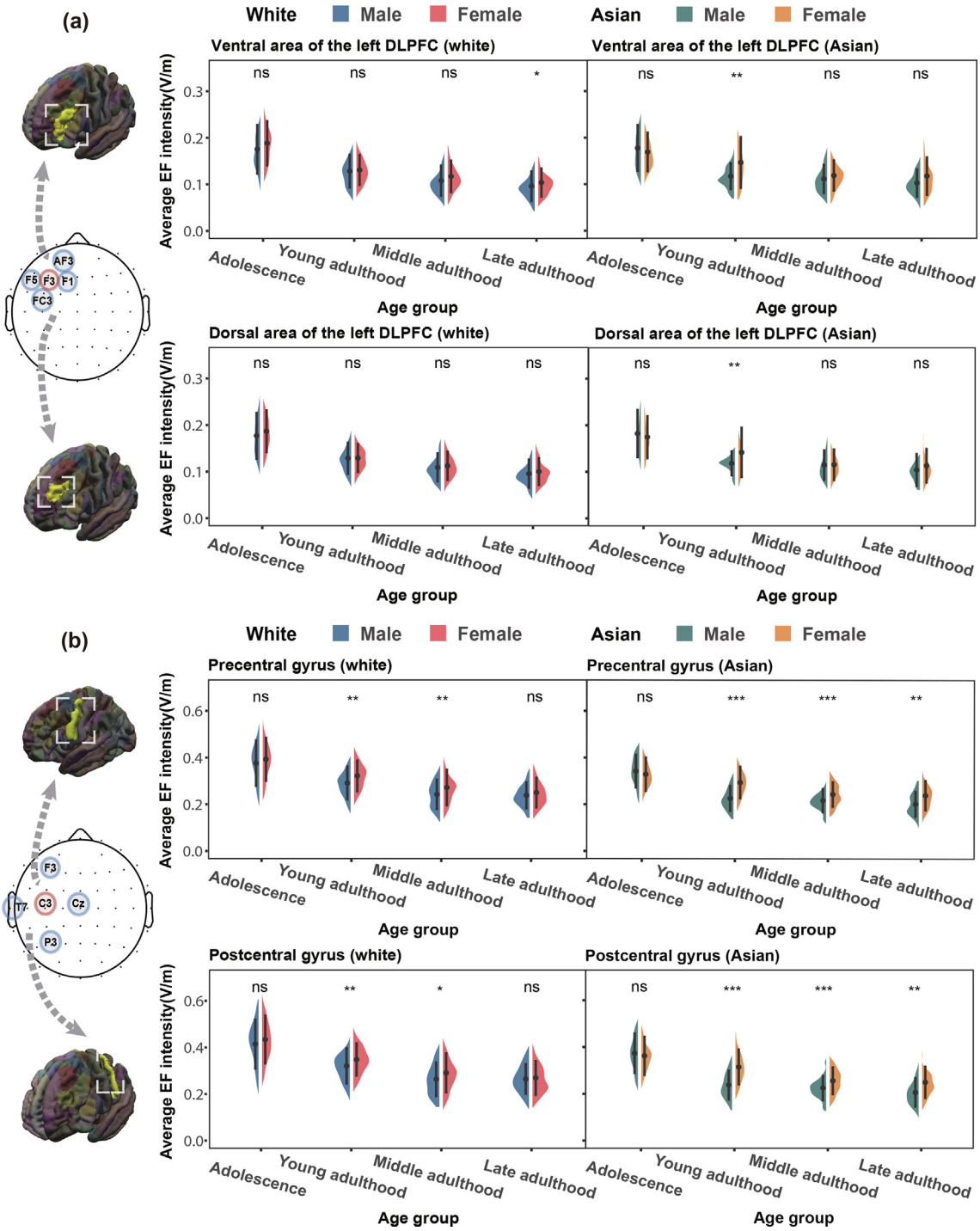

Fig. 2. Violin plots of EF intensity averages and standard deviations in ROIs by age group, gender and ethnicity (in V m^{-1}). The first column on the left illustrates the electrode positions and ROIs for two montages. Stimulation intensity on the electrodes is represented by red (2 mA) and blue (0.5 mA) for transcranial electrical stimulation. Asterisks denote statistically significant effects: *P<0.05, **P<0.01, ***P<0.001. (a) Simulated EF intensity in ROIs for tES over DLPFC. In both ROIs of the DLPFC, the EF intensities of adolescents were significantly higher compared to other age groups. Gender differences were significant in Asian young adults after FDR correction. (b) Simulated EF intensity in ROIs for tES over the motor cortex. For both ROIs of the motor cortex, the EF intensities of adolescents were significantly higher compared to other age groups. Gender differences were significant in young and middle adulthood as well as Asian late adulthood. EF: electric field; ROI: region of interest; DLPFC: dorsolateral prefrontal cortex; tES: transcranial electrical stimulation; ns: not significant.

effect of gender in all ROIs (P_{gender}<0.01), except for the dorsal area of DLPFC (P_{gender}>0.05 for both races). Interaction effects of age and gender were found only among the Asian groups (Table 1). Further multiple comparisons revealed that the most significant age-related intensity decrease occurred in young adults compared to the adolescent group in both ethnic groups, whereas the least significant age-related difference was between the elderly and the middle-aged groups. In all populations except male Asians, the motor cortex montage exhibited a greater intensity decrease in the middle-aged group compared to young adults (P<1×10^{-5}, FDR corrected across brain regions and demographic groups), whereas the DLPFC montage showed a less significant intensity

Table 1
ANOVA results of electric field intensity in the white and the Asian cohort.

	White				Asian			
	DLPFC		Motor		DLPFC		Motor	
	Ventral area	Dorsal area	Postcentral	Precentral	Ventral area	Dorsal area	Postcentral	Precentral
F_{gender}	10.9	3.72	12.2	20.1	10.2	2.84	36.4	32.8
P_{gender}	9.82×10^{-4}	0.0542	5.02×10^{-4}	8.40×10^{-6}	1.50×10^{-3}	0.0927	2.84×10^{-9}	1.59×10^{-8}
F_{age}	221	262	184	173	93	79	130	111
P_{age}	8.43×10^{-108}	6.99×10^{-123}	2.30×10^{-93}	7.12×10^{-89}	3.54×10^{-49}	3.58×10^{-43}	7.18×10^{-65}	3.67×10^{-57}
$F_{gender \times age}$	0.747	0.659	1.11	0.957	5.87	4.37	10.6	11.5
$P_{gender \times age}$	0.524	0.577	0.342	0.412	5.90×10^{-4}	4.70×10^{-3}	8.14×10^{-7}	2.62×10^{-7}

ROI: region of interest; DLPFC: dorsolateral prefrontal cortex.

decrease (P<0.05, FDR corrected). Notably, there were no significant intensity decreases in the middle-aged group compared to young adults for either montage in male Asians. Regarding gender differences, few significant gender-related differences were observed for the DLPFC montage, except for Asian young adults. However, significant gender-related differences were found for the motor cortex montage, except for adolescent groups and the white elderly (Table S2 in Supplementary materials).

Given the observed association between intensities and age at the group level, we performed an age correlation analysis (Fig. S1 in Supplementary materials) and established GAMs to derive fitted age trajectories (Fig. 3). Consistent with group-level differences, all age trajectories exhibited a clear declining trend over time with sharp decreases until around age 25, followed by a flattening out of the intensity declines. Regarding gender differences, separate smooth curves estimated for males and females indicated higher overall intensities in females, as mentioned earlier, and greater gender differences for the motor cortex montage (P<0.001 in both ROIs of the motor cortex montage for both ethnic groups) compared to the DLPFC montage. It is noteworthy that the age trajectories for the females had relatively gentler slopes than those for males, especially during adolescence and early adulthood in the Asian population for the motor cortex montage. When comparing the nonlinear relationships between EF intensities and age for different montages and different ethnic cohorts, we observed significant interaction effects of age and gender only in the Asian (ventral area of DLPFC, F=3.09, P=0.00887; postcentral gyrus, F=5.96, P=1.03×10^{-6}; precentral gyrus, F=5.23, P=1.34×10^{-5}). The fitted curves indicated that received intensities in Asian males were slightly higher than in Asian females during early adolescence, with the point of intersection occurring at around age 18. We also validated these findings using the AAL3 atlas and generalized them to the right-hemispheric region. Results in detail are provided in the Supplementary material (Note S3–S4, Fig. S2–S3 online).

Additionally, we computed the focality of the selected montages to assess individual differences in focality of electrical stimulation across eight demographic groups. Two-way ANOVA revealed significant main effects of age in both ethnic cohorts for both montages. Detailed analysis procedure and results can be found in Supplementary materials (Note S1–S2 online).

3.2. Key anatomical factors underlying the inter-individual variability

Using the same dataset of 1616 structural MRI scans, we then aimed to explore the anatomical factors underlying the individual variability observed in tES-induced EF distribution across demographic groups in Study 2. We performed stepwise linear regression, considering all 9 anatomical features for each montage within each ethnic cohort, with intensity or focality as the dependent variable. No variables were excluded in backward elimination for intensities. Table S3 in Supplementary materials presents the intensity outcomes for the ROI with the greater intensity in each montage, given that the two selected ROIs exhibited similar results. The findings regarding focality are available in the Supplementary materials (Note S2 online). The intensity outcomes demonstrated that all anatomical variables accounted for 75.8%–84.4% of the variance in intensity.

Local scalp thickness (P<0.0001 for all groups), local skull thickness (P<0.0001 for all groups), and local epidural CSF thickness (P<0.0001 for all groups) emerged as the dominant factors in explaining inter-individual variability. These anatomical factors showed significant negative correlations with intensity (P<0.0001 for all groups; upper panel of Fig. 4b). Cortical thickness and LGI were also influential factors in most groups. Brain volume showed positive correlations for the DLPFC montage and negative correlations for the motor cortex montage, whereas ROI-anode distance exhibited negative correlations for the DLPFC montage and positive correlations for the motor cortex montage. The lower panel of Fig. 4b presents the calculated effect size (Cohen's f^2) for each feature under different conditions, quantifying the contribution of each anatomical factor to individual differences in intensity. Among these factors, skull thickness emerged as the most influential (f^2>1.2 for all groups), followed by scalp thickness (f^2>0.35 for all groups) and CSF thickness. Notably, CSF thickness appeared more important in the Asian cohort (f^2>0.35 for both montages) compared to the white cohort. To understand how anatomical factors explain the differences in EF trends with age across ethnicities, we also fitted age trajectories of local scalp thickness, skull thickness, and CSF thickness. In particular, variations in skull thickness and its direct correlation with EF intensity across different age groups were comprehensively investigated. These results can be found in the Supplementary materials (Note S5, Fig. S6–S8, Table S8 online).

Next, we constructed multivariate models incorporating scalp thickness, skull thickness, and CSF thickness, the three pivotal elements considered most predictive of the intensity outcomes. The linear predictors estimated EF intensities with *MAE* (mean absolute error) ranging from 0.0157 to 0.0376 V m^{-1} and explained variance (adjusted R^2) between 72.1% and 81.0% (*MAE*=0.0157, adjusted R^2=0.810 for the DLPFC montage in the white cohort; *MAE*=0.0186, adjusted R^2=0.736 for the DLPFC montage in the Asian cohort; *MAE*=0.0368, adjusted R^2=0.787 for the motor cortex montage in the white cohort; *MAE*=0.0376, adjusted R^2=0.721 for the motor cortex montage in the Asian cohort).

3.3. Coupling of simulated electric fields and actual brain activations

Next, we investigated the association between simulated EF and changes in brain activity induced by HD-tDCS targeting left OFC in Study 3. By comparing distances between the real and sham stimulation groups, we assessed the effects of tDCS on brain activations (Fig. 5a).

We mapped the maximum EF intensity sites and maximum fALFF/DC change sites of all participants from both groups onto

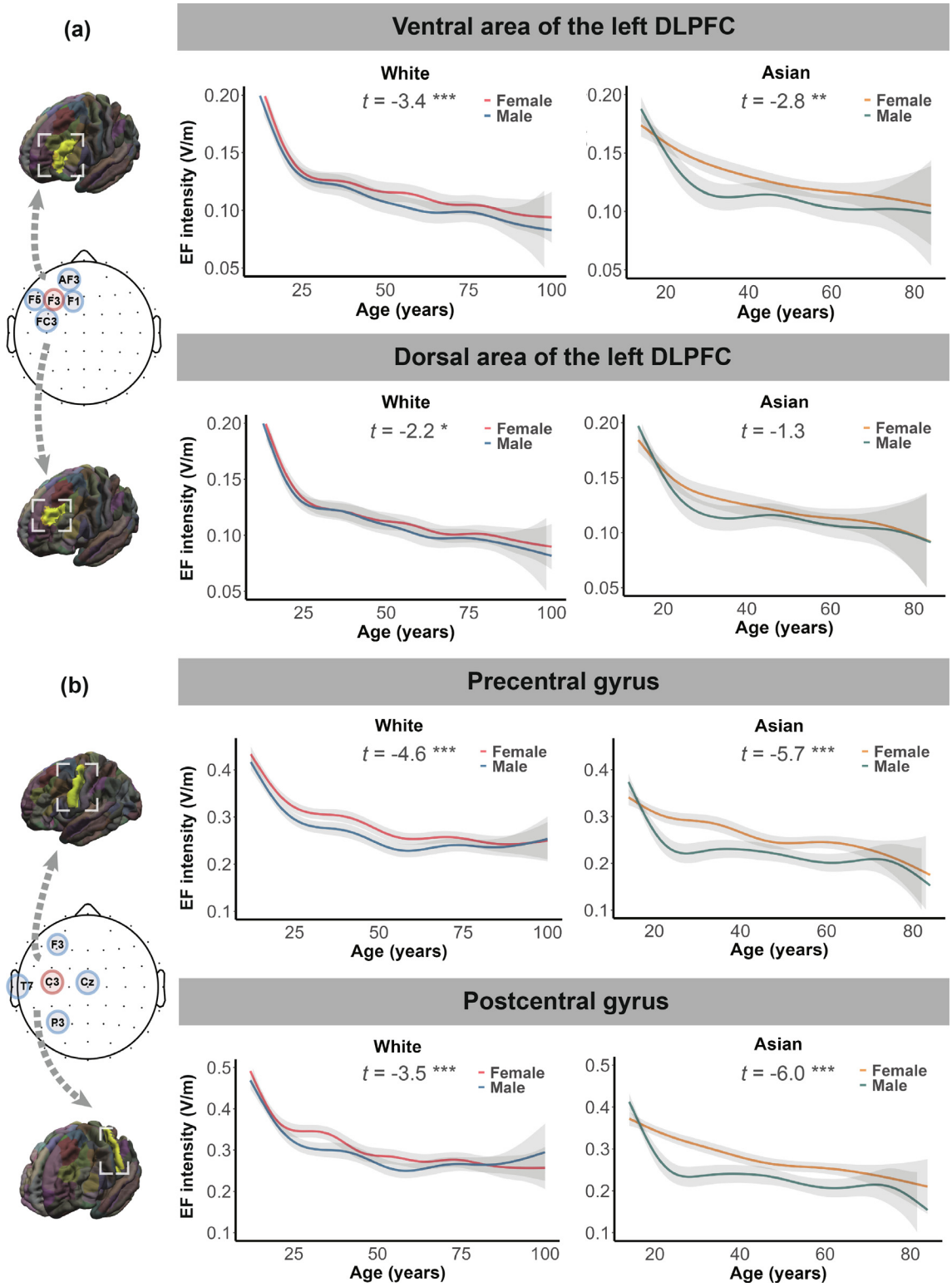

Fig. 3. Fitted age trajectories of EF intensity in ROIs by gender and ethnicity (in V/m). Stimulation intensities were set to 2mA at the central electrode and 0.5mA at the return electrodes for transcranial electrical stimulation. The shaded regions denote 95% CI. The intercept difference (gender difference: male-female) for EF intensity is shown above each trajectory, including both t-value and significance. Asterisks denote statistically significant effects: *P<0.05, **P<0.01, ***P<0.001. (a) Fitted age trajectories for tES over DLPFC. (b) Fitted age trajectories for tES over the motor cortex. EF: electric field; ROI: region of interest; CI: confidence interval; DLPFC: dorsolateral prefrontal cortex; tES: transcranial electrical stimulation.

template brain surfaces, as depicted in Fig. 5b. We observed that maximum intensity sites were concentrated in two specific brain regions near the target area. In contrast, the maximum fALFF/DC changes were dispersed throughout the OFC region for both the real tDCS and sham groups. Compared to DC, maximum fALFF change sites were more concentrated in the left hemisphere, with

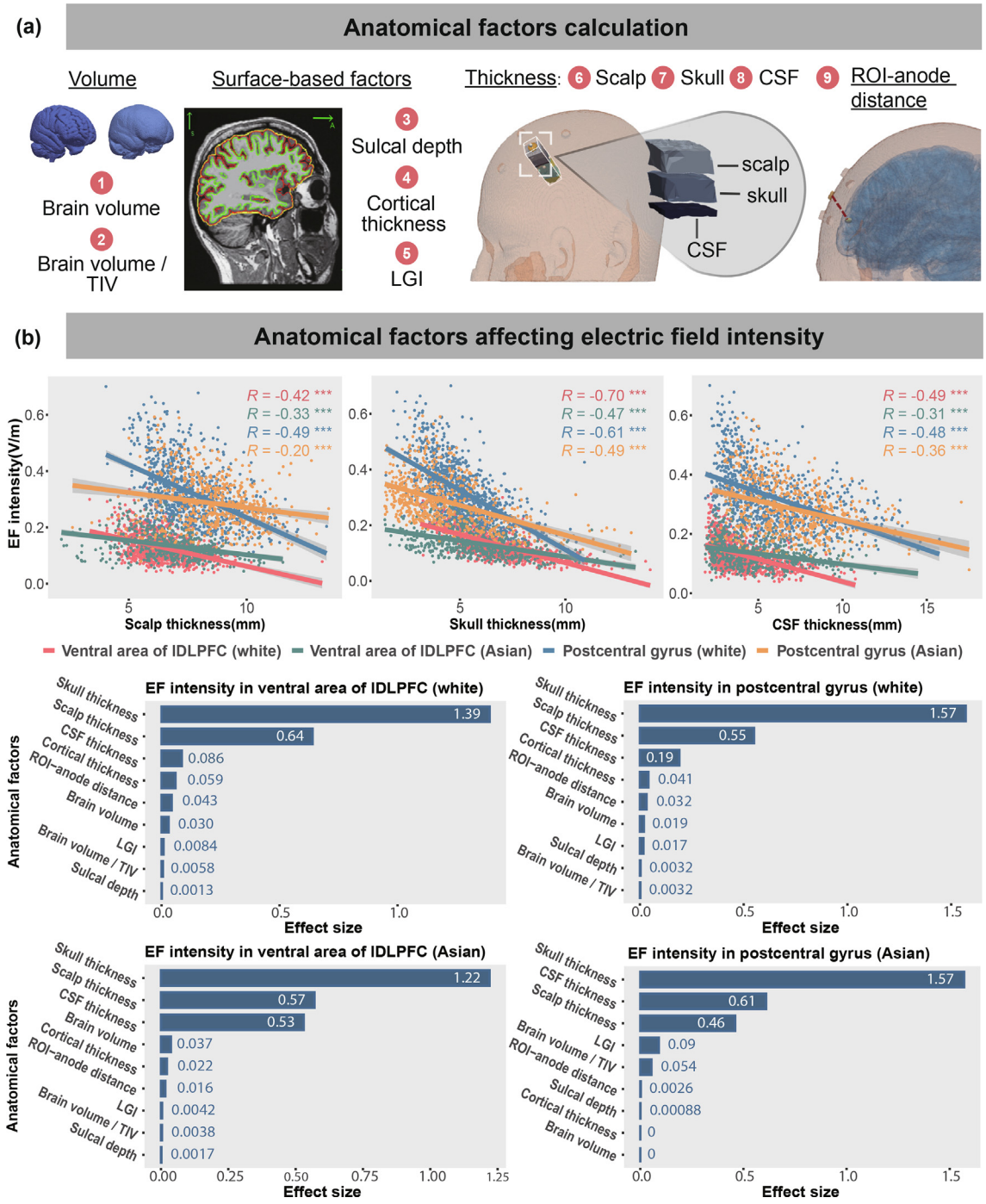

Fig. 4. Key anatomical factors that explain the variability in the tES-induced EF intensity. (a) Illustration of nine anatomical features. These features were selected based on head anatomy and VIF values (VIF<4) to minimize multicollinearity between variables. (b) Impact of anatomical factors on the EF intensities in ROIs. The anatomical factors are sorted by effect size (Cohen's f^2). The bars indicate that skull thickness, scalp thickness and CSF thickness are the most significant factors affecting EF intensity within the target cortical regions. The lower panel displays scatterplots for these three factors, with individual participants represented by dots grouped by ethnicity and montage. Fitting regression lines are superimposed with the shaded portion denoting SE. Asterisks indicate significant correlations between electric field intensity and each of the three factors for all groups. ROI: region of interest; LGI: local gyrification index; TIV: total intracranial volume; CSF: cerebrospinal fluid; lDLPFC: left dorsolateral prefrontal cortex; EF: electric field; VIF: variance inflation factor; tES: transcranial electrical stimulation.

greater overlap across participants in the real tDCS group than in the sham group. Additionally, independent two-tailed t-tests revealed a significant difference (sham-tDCS: t=2.99, P=0.00482) between the two groups in the distance between the targeted region and the region with the largest fALFF changes during stimulation (Fig. 5c). The increased consistency of maximum activations and the decreased distances in the real tDCS group compared to the sham group provide evidence of the immediate tDCS effects on local spontaneous brain activity. However, no statistically significant effects were observed in post-stimulation analyses (sham-tDCS: t=0.118, P=0.855) (Fig. 5c). Functional connectivity analyses also indicated no significant differences between the sham and tDCS groups in terms of the distances between the region with the maximum EF intensity and the subregion within

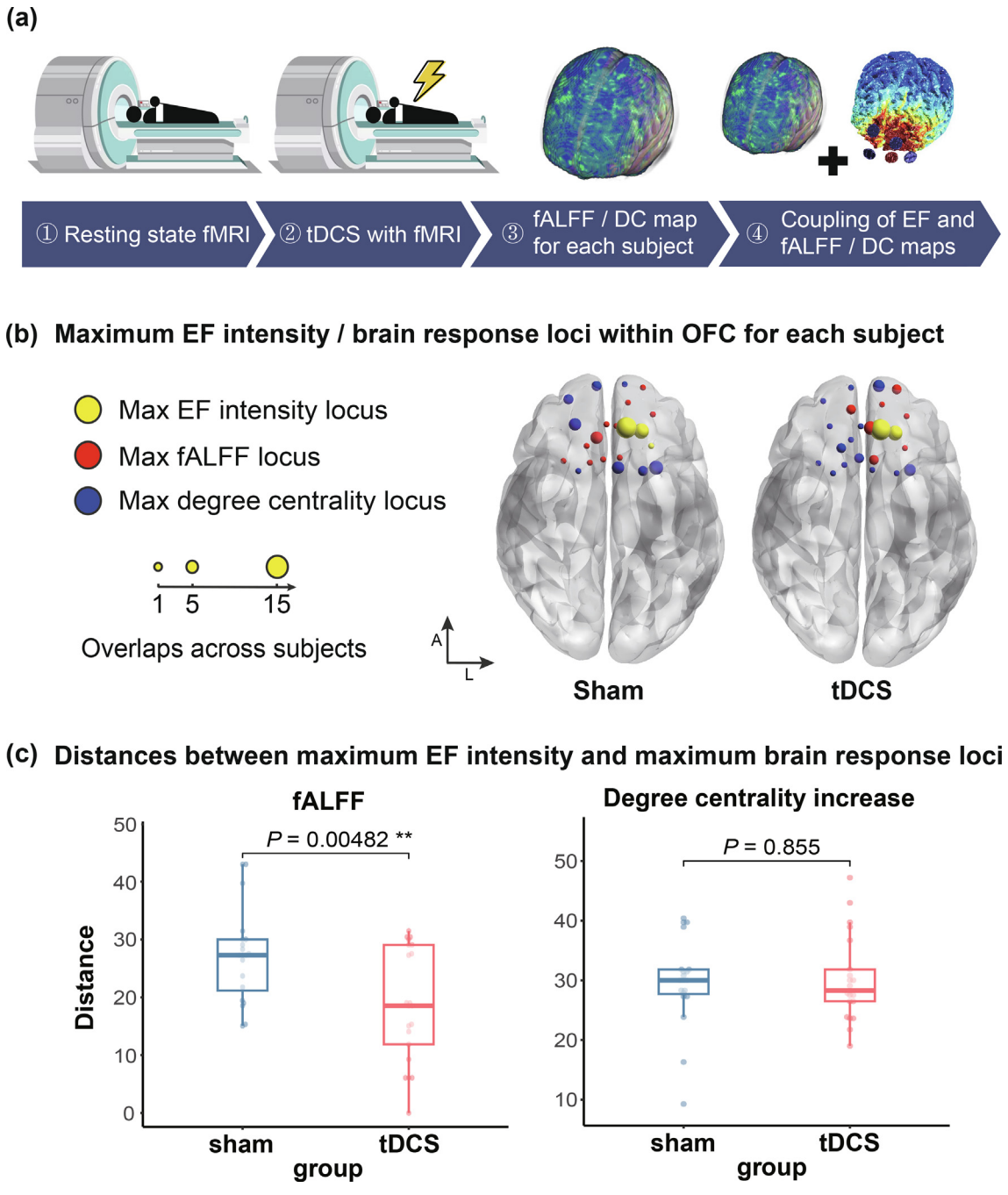

Fig. 5. Coupling of simulated EF and actual brain activations. (a) Workflow of neuromodulation fMRI and data analysis. Electrical stimulation was applied over OFC with a central electrode at Fp1(1.5 mA) and return electrodes at Fpz (−0.375 mA), AFz (−0.375 mA), AF3 (−0.375 mA), and AF7 (−0.375 mA). (b) Maximum EF intensity locus and maximum brain response locus within OFC for each participant. Brain regions were defined based on the 800 parcellation Schaefer atlas with a focus on the OFC. The yellow balls indicate the center of the brain region with maximum EF intensity for each individual, while the red balls and the blue balls indicate the center of the brain region with maximum fALFF changes and maximum DC increases respectively. Ball size reflects the number of participants sharing the particular locus. (c) tDCS effects on the coupling of tDCS-induced EF and brain response during stimulation. Distances between the maximum EF intensity locus and maximum brain response locus were calculated for each individual. Distance in the tDCS group was significantly shorter than in the sham group. tDCS: transcranial direct current stimulation; fALFF: fractional ALFF; DC: degree centrality; fMRI: functional magnetic resonance imaging; EF: electric field; OFC: orbitofrontal cortex; A: anterior; L: left.

the orbitofrontal area showing the most pronounced increase in DC both during stimulation (sham-tDCS: t=-0.183, P=0.855) and after stimulation (sham-tDCS: t=1.29, P=0.204). We observed a lower mean and higher variance in distance for post-stimulation effects compared to during-stimulation effects. The visualization of post-stimulation effects, as measured by fALFF and DC, can be found in the Supplementary material (Fig. S9 online).

3.4. A transcranial electric field simulation toolbox with ready-made head models

The age and gender differences observed in intensities of EF induced by tES in Study 1, along with the age-dependent tES focality, underscore the importance of considering anatomical traits of diverse populations across age, gender and ethnicity in tES-

related studies. Therefore, we developed tESview, a toolbox designed to enable efficient and cost-effective EF calculations for any given montage. The toolbox includes a library of head models representing multiple demographic cohorts (white and Asian) at different ages, ensuring an accurate representation of these specific demographic groups. The resulting EF applies to both tDCS and transcranial alternating current stimulation under 1 kHz. Details and implementation of the toolbox can be found in the Supplementary materials (Note S6 online).

4. Discussion

In this study, we investigated how EF intensity varies across the lifespan and among different populations, and how it relates to the neural effects of tES. First, we used MRI-guided FEM to chart the lifespan changes of EF intensity. We found that EF intensity decreased significantly with age, especially before the age of 25. Gender and ethnicity were also found to influence EF intensity, with females exhibiting higher intensities in the target regions compared to males, and Asians showing slightly lower EF intensity than whites. Second, we estimated how anatomical factors contributed to the differences in EF intensity among individuals. We showed that local skull thickness, local scalp thickness, and local epidural CSF thickness were major contributors. Finally, we used concurrent tES-fMRI to observe the neural responses to electrical stimulation at the individual level and demonstrated associations between the simulated EF and the brain activity changes induced by tES. We concluded the study by providing an open-source toolbox featuring age-stratified head models for efficient EF calculations.

With a focus on HD-tES, our study builds upon previous research on bipolar montages. We confirmed the decline in EF intensities with age and provided a finer characterization of age-related trends. Supplementary analyses proved the reliability of our findings using different brain parcellation methods and suggested that these findings could also apply to contralateral regions. Considering multiple anatomical factors, we identified local skull thickness as a critical factor negatively correlated with intensities, particularly between the ages of 12 and 25. Previous findings revealed that skull thickness significantly increased with age until early adulthood in the white group [64–66]. This evidence suggests that changes in skull thickness may contribute to the rapid decline in EF intensity before the age of 25. Moreover, we found that intensities in ROIs for the DLPFC montage were considerably lower compared to those for the motor cortex montage, potentially attributed to the greater thickness of frontal bones compared to parietal bones [67]. These findings supplement the conventional assumption that increased CSF associated with aging or neurological disorders, is the primary factor explaining the intensity decrease with age.

It is also important to consider individual differences in the focality of tES electric field, as previous research has suggested that HD-tES, with its increased focality, is more sensitive to variations in head anatomy than conventional bipolar montages [68]. A prior study employing area-based metrics demonstrated a significant impact of gray matter volume on focality under a bipolar montage [20]. However, area-based metrics are substantially influenced by the participant's brain size. To address this issue, we used relative-area metrics, dividing the surface area of the stimulated region by the total area of the corresponding hemisphere. Our findings on HD-tES focality identified scalp thickness and cortical thickness as significant influencing factors, though these results were not entirely consistent across ethnic groups. Importantly, the definition of tES focality varies greatly among existing studies [69–74]. Further research is needed to standardize the use of focality metrics.

A comprehensive examination of various anatomical factors and the identification of key components can greatly contribute to the development of predictive models for EF intensity. For example, our linear regression model, considering three dominant factors (i.e., skull thickness, scalp thickness, and epidural CSF thickness), yielded accurate predictions, with explained variance and *MAE* comparable to the model incorporating all nine anatomical factors. Notably, acquiring measurements of the three tissue thicknesses is more time-efficient than obtaining all nine factors. Therefore, elucidating these key factors enables more efficient predictions of EF intensities in the target region based on individuals' primary anatomical characteristics.

In addition to computational modeling, fMRI recordings during tES provide insights into individual differences in resting-state neural activities in response to electrical stimulation. By visualizing the regions with maximum EF intensities simulated for each participant and the locations of maximum brain activity changes during stimulation, we observed that, compared to the sham group, the active tDCS group had more participants with the strongest brain activation near the orbitofrontal region, which coincided with the most stimulated region identified by simulation. This confirmed the spatial consistency between the actual brain activation and the simulated EF, indicating that tES simulation could reflect tES-induced brain activity changes in the target region. This consistency was not observed in functional connectivity or post-stimulation measures. The absence of fALFF post-stimulation effect possibly indicated a diminished tDCS effect on local brain activities after stimulation. The scattered distribution of maximum brain activations across individuals suggested that tES-induced functional responses could exhibit significant inter-individual variability, particularly in degree centrality. Inappropriate tES doses and settings may further amplify this variability, compromising the validity and sensitivity of tES studies.

Although our main results were obtained from the healthy population, it is important to note that these findings could apply to patient populations. As an exploratory analysis, we obtained MRI data from Alzheimer's disease (AD) patients and healthy controls, and then simulated EFs induced by tES targeting the left DLPFC. We demonstrated that the EF intensities and focality obtained from healthy controls could generalize to AD patients, and that regression models established based on the healthy population, including the reduced model including only three tissue thickness factors, are also applicable to AD patients. Details of the analyses are available in the Supplementary materials (Note S7, Fig. S10 online). The results suggest that structural brain changes associated with AD did not significantly affect intracranial electric field intensity. Future studies need to include diverse patient populations (e.g., depression) and larger sample sizes to identify the potential clinical applications of our EF modeling for neuropsychiatric disorders.

TES-induced EF intensity and distribution vary significantly across different age and ethnic populations, highlighting the importance of individualized EF modeling. However, considering the high cost of MRI acquisition for each individual, it is practical to stratify populations based on demographic variables such as age, gender, and ethnicity to establish standard head models for tES at the group level. The toolbox that we developed for this purpose includes head models of both the white cohort and the Asian cohort, stratified by age. Furthermore, identifying key anatomical factors underlying individual differences in tES-induced EF opens up possibilities for constructing predicative models relating major anatomical factors to EF intensity. These efforts can advance the practical application of individualized tES research.

There are several limitations in the current study. First, comparisons between ethnic groups may be influenced by site effects, since the data batches were obtained from distinct sources. To verify the reliability of our conclusions, we performed additional analyses demonstrating that the simulation results were minimally

affected by the scanning environment. Results of these site effect analyses are presented in the Supplementary materials (Note S8 online). Second, we used fixed values for conductivities to reduce confounders in the analysis of head tissue morphologies. Thus, anisotropy of tissues such as white matter and age-related changes in conductivity for different tissues were not accounted for. For example, the conductivity of the skull, a major tissue affecting the EF, is known to decrease with age [67]. Considering this change would likely reveal a more pronounced decline in EF intensity with age. Additionally, different regions of the skull tissue might possess varying densities and conductivities, although the frontal bone and parietal bones, relevant to this research, exhibit similar compositions [67]. Lastly, the functional aspects examined in Study 3 focused solely on the overall intensity of brain activations during stimulation, leaving the dynamic process of brain activity changes unknown.

5. Conclusion

In conclusion, we demonstrated how the electric field of high-definition tES varies across the lifespan in both white and Asian populations, and its association with tES-induced neural responses measured by fMRI. Our study provided an open-source toolbox featuring age-stratified head models for efficient EF calculations. Thus, these findings offer a detailed characterization of individual differences in tES-induced EF and provide a resource for conducting personalized neuromodulation.

Conflict of interest

YH is an employee of Soterix Medical, Inc., but does not have any competing interest related to this study. The other authors declare no conflict of interest.

Acknowledgments

This work was supported by the National Natural Science Foundation of China (32171078 and 32322035), STI2030-Major Projects by the Ministry of Science and Technology of China (2022ZD0206400), Scientific Foundation of the Institute of Psychology, Chinese Academy of Sciences (E0CX52 and E2CX4015), and Young Elite Scientist Sponsorship Program by the China Association for Science and Technology (E1KX0210). Data were provided in part by the Human Connectome Project, WU-Minn Consortium (Principal Investigators: David Van Essen and Kamil Ugurbil; 1U54MH091657) funded by the 16 NIH Institutes and Centers that support the NIH Blueprint for Neuroscience Research; and by the McDonnell Center for Systems Neuroscience at Washington University.

Author contributions

Yiheng Tu designed and supervised the research. He also contributed to funding acquisition and project administration. Weiwei Ma and Yiheng Tu contributed to methodology of the research, visualization of the results, and writing of the original draft. Weiwei Ma, Feixue Wang, and Yangyang Yi performed data analysis and the experiments. Xinying Li, Yaou Liu, and Yiheng Tu also contributed to data acquisition and investigation. Weiwei Ma, Yu Huang, Yaou Liu, and Yiheng Tu contributed to review and editing of the draft.

Data availability and code availability

The HCP data is publicly available at https://www.humanconnectome.org/study/hcp-young-adult and NIMH Data Archive - CCF (nih.gov). The library of head models for multiple demographic cohorts mentioned in the Results section is publicly available at https://github.com/tulab-brain/tESview/releases/tag/v1.0.

The ROAST software is publicly available at www.parralab.org. The open-source toolbox tESview can be downloaded from the same link where the head models are available.

Appendix A. Supplementary material

Supplementary data to this article can be found online at https://doi.org/10.1016/j.scib.2024.10.001.

References

[1] Antal A, Alekseichuk I, Bikson M, et al. Low intensity transcranial electric stimulation: Safety, ethical, legal regulatory and application guidelines. Clin Neurophysiol 2017;128:1774–809.
[2] Bikson M, Brunoni AR, Charvet LE, et al. Rigor and reproducibility in research with transcranial electrical stimulation: An NIMH-sponsored workshop. Brain Stimul 2018;11:465–80.
[3] Li ZJ, Zhang LB, Chen YX, et al. Advancements and challenges in neuromodulation technology: Interdisciplinary opportunities and collaborative endeavors. Sci Bull 2023;68:1978–82.
[4] Horvath JC, Forte JD, Carter O. Evidence that transcranial direct current stimulation (tDCS) generates little-to-no reliable neurophysiologic effect beyond MEP amplitude modulation in healthy human subjects: A systematic review. Neuropsychologia 2015;66:213–36.
[5] Zanto TP, Jones KT, Ostrand AE, et al. Individual differences in neuroanatomy and neurophysiology predict effects of transcranial alternating current stimulation. Brain Stimul 2021;14:1317–29.
[6] Terranova C, Rizzo V, Cacciola A, et al. Is there a future for non-invasive brain stimulation as a therapeutic tool? Front Neurol 2018;9:1146.
[7] Datta A, Bansal V, Diaz J, et al. Gyri-precise head model of transcranial direct current stimulation: Improved spatial focality using a ring electrode versus conventional rectangular pad. Brain Stimul 2009;2:201–7.
[8] Miranda PC, Lomarev M, Hallett M. Modeling the current distribution during transcranial direct current stimulation. Clin Neurophysiol 2006;117:1623–9.
[9] Oostendorp TF, Hengeveld YA, Wolters CH, et al. Modeling transcranial DC stimulation. 30th Annual International IEEE EMBS Conference 2008.
[10] Wagner T, Fregni F, Fecteau S, et al. Transcranial direct current stimulation: A computer-based human model study. Neuroimage 2007;35:1113–24.
[11] Bethlehem RAI, Seidlitz J, White SR, et al. Brain charts for the human lifespan. Nature 2022;604:525–33.
[12] Caspi Y, Brouwer RM, Schnack HG, et al. Changes in the intracranial volume from early adulthood to the sixth decade of life: A longitudinal study. Neuroimage 2020;220:116842.
[13] Frank K, Gotkin RH, Pavicic T, et al. Age and gender differences of the frontal bone: A computed tomographic (CT)-based study. Aesthet Surg J 2019;39:699–710.
[14] Tang Y, Zhao L, Lou Y, et al. Brain structure differences between Chinese and Caucasian cohorts: A comprehensive morphometry study. Hum Brain Mapp 2018;39:2147–55.
[15] Urban JE, Weaver AA, Lillie EM, et al. Evaluation of morphological changes in the adult skull with age and sex. J Anat 2016;229:838–46.
[16] Bikson M, Rahman A, Datta A, et al. High-resolution modeling assisted design of customized and individualized transcranial direct current stimulation protocols. Neuromodulation 2012;15:306–15.
[17] Huang Y, Datta A, Bikson M, et al. Realistic volumetric-approach to simulate transcranial electric stimulation-roast-a fully automated open-source pipeline. J Neural Eng 2019;16:056006.
[18] Lee C, Jung Y-J, Lee SJ, et al. Comets2: An advanced MATLAB toolbox for the numerical analysis of electric fields generated by transcranial direct current stimulation. J Neurosci Methods 2017;277:56–62.
[19] Saturnino GB, Puonti O, Nielsen JD. SimNIBS 2.1: A comprehensive pipeline for individualized electric field modelling for transcranial brain stimulation. In: Makarov S, Horner M, Noetscher G, editors. Brain and Human Body Modeling. Cham: Springer; 2019. p. 3–25.
[20] Antonenko D, Grittner U, Saturnino G, et al. Inter-individual and age-dependent variability in simulated electric fields induced by conventional transcranial electrical stimulation. Neuroimage 2021;224:117413.
[21] Bhattacharjee S, Kashyap R, Goodwill AM, et al. Sex difference in tDCS current mediated by changes in cortical anatomy: A study across young, middle and older adults. Brain Stimul 2022;15:125–40.
[22] Ciechanski P, Carlson HL, Yu SS, et al. Modeling transcranial direct-current stimulation-induced electric fields in children and adults. Front Hum Neurosci 2018;12:268.
[23] Hunold A, Haueisen J, Freitag CM. Cortical current density magnitudes during transcranial direct current stimulation correlate with skull thickness in children, adolescent and young adults. In: Kadosh R, Zaehle T, Krauel K, editors. Progress in brain research. Academic Press, Inc; 2021. p. 41–56.
[24] Indahlastari A, Albizu A, O'Shea A, et al. Modeling transcranial electrical stimulation in the aging brain. Brain Stimul 2020;13:664–74.

[25] Laakso I, Tanaka S, Koyama S, et al. Inter-subject variability in electric fields of motor cortical tDCS. Brain Stimul 2015;8:906–13.
[26] Rezaee Z, Dutta A. Lobule-specific dosage considerations for cerebellar transcranial direct current stimulation during healthy aging: A computational modeling study using age-specific magnetic resonance imaging templates. Neuromodulation 2020;23:341–65.
[27] Russell M, Goodman T, Wang Q, et al. Gender differences in current received during transcranial electrical stimulation. Front Psychiatry 2014;5:104.
[28] Thomas C, Datta A, Woods A. Effect of aging on cortical current flow due to transcranial direct current stimulation: Considerations for safety. In: Proceedings of the 40th Annual International Conference of the IEEE-Engineering-in-Medicine-and-Biology-Society (EMBC), Honolulu, HI, JUL 18-21, 2018.
[29] Thomas C, Ghodratitoostani I, Delbem ACB, et al. Influence of gender-related differences in transcranial direct current stimulation: A computational study. In: Proceedings of the 41st Annual International Conference of the IEEE-Engineering-in-Medicine-and-Biology-Society (EMBC), Berlin, GERMANY, JUL 23-27, 2019.
[30] Im C, Seo H, Jun SC. Geometrical variation's influence on the effects of stimulation may be important in the conventional and multi-array tDCS–comparison of electrical fields computed. IEEE Access 2019;7:8557–69.
[31] Opitz A, Paulus W, Will S, et al. Determinants of the electric field during transcranial direct current stimulation. Neuroimage 2015;109:140–50.
[32] Filmer HL, Ehrhardt SE, Shaw TB, et al. The efficacy of transcranial direct current stimulation to prefrontal areas is related to underlying cortical morphology. Neuroimage 2019;196:41–8.
[33] Lu H, Lam LCW, Ning Y. Scalp-to-cortex distance of left primary motor cortex and its computational head model: Implications for personalized neuromodulation. CNS Neurosci Ther 2019;25:1270–6.
[34] Mahdavi S, Towhidkhah F. Alzheimer's disease neuroimaging I. Computational human head models of tDCS: Influence of brain atrophy on current density distribution. Brain Stimul 2018;11:104–7.
[35] Mosayebi-Samani M, Jamil A, Salvador R, et al. The impact of individual electrical fields and anatomical factors on the neurophysiological outcomes of tDCS: A TMS-MEP and MRI study. Brain Stimul 2021;14:316–26.
[36] Datta A, Zhou X, Su Y, et al. Validation of finite element model of transcranial electrical stimulation using scalp potentials: Implications for clinical dose. J Neural Eng 2013;10:036018.
[37] Datta A, Krause MR, Pilly PK, et al. On comparing in vivo intracranial recordings in non-human primates to predictions of optimized transcranial electrical stimulation. In: Proceedings of the 38th Annual International Conference of the IEEE-Engineering-in-Medicine-and-Biology-Society (EMBC), Orlando, FL, 2016.
[38] Huang Y, Liu AA, Lafon B, et al. Measurements and models of electric fields in the in vivo human brain during transcranial electric stimulation. Elife 2017;6:e18834.
[39] Puonti O, Saturnino GB, Madsen KH, et al. Value and limitations of intracranial recordings for validating electric field modeling for transcranial brain stimulation. Neuroimage 2020;208:116431.
[40] Antal A, Bikson M, Datta A, et al. Imaging artifacts induced by electrical stimulation during conventional fMRI of the brain. Neuroimage 2014;85(Pt 3):1040–7.
[41] Ekhtiari H, Ghobadi-Azbari P, Thielscher A, et al. A checklist for assessing the methodological quality of concurrent tES-fMRI studies (contes checklist): A consensus study and statement. Nat Protoc 2022;17:596–617.
[42] Esmaeilpour Z, Shereen AD, Ghobadi-Azbari P, et al. Methodology for tDCS integration with fMRI. Hum Brain Mapp 2020;41:1950–67.
[43] Meinzer M, Lindenberg R, Darkow R, et al. Transcranial direct current stimulation and simultaneous functional magnetic resonance imaging. J Vis Exp 2014;86:e51730.
[44] Nardo D, Creasey M, Negus C, et al. Transcranial direct current stimulation with functional magnetic resonance imaging: A detailed validation and operational guide. Wellcome Open Res 2021;6:143.
[45] Saiote C, Turi Z, Paulus W, et al. Combining functional magnetic resonance imaging with transcranial electrical stimulation. Front Hum Neurosci 2013;7:435.
[46] Lu B, Chen X, Xavier Castellanos F, et al. The power of many brains: Catalyzing neuropsychiatric discovery through open neuroimaging data and large-scale collaboration. Sci Bull 2024;69:1536–55.
[47] Harms MP, Somerville LH, Ances BM, et al. Extending the human connectome project across ages: Imaging protocols for the lifespan development and aging projects. Neuroimage 2018;183:972–84.
[48] Van Essen DC, Smith SM, Barch DM, et al. The WU-Minn Human Connectome Project: An overview. Neuroimage 2013;80:62–79.
[49] Glasser MF, Sotiropoulos SN, Wilson JA, et al. The minimal preprocessing pipelines for the human connectome project. Neuroimage 2013;80:105–24.
[50] Kvasnak E. Perception and pain thresholds of tDCS and tACS. Physiol Res 2019;68:S427–31.
[51] Kang HJ, Kawasawa YI, Cheng F, et al. Spatio-temporal transcriptome of the human brain. Nature 2011;478:483–9.
[52] Fan L, Li H, Zhuo J, et al. The human brainnetome atlas: A new brain atlas based on connectional architecture. Cereb Cortex 2016;26:3508–26.
[53] Dale AM, Fischl B, Sereno MI. Cortical surface-based analysis. I Segmentation and surface reconstruction. Neuroimage 1999;9:179–94.
[54] Fischl B, Dale AM. Measuring the thickness of the human cerebral cortex from magnetic resonance images. Proc Natl Acad Sci USA 2000;97:11050–5.
[55] Schaer M, Cuadra MB, Tamarit L, et al. A surface-based approach to quantify local cortical gyrification. IEEE Trans Med Imaging 2008;27:161–70.
[56] Ahrens J, Geveci B, Law C. Paraview: An end-user tool for large data visualization, visualization handbook. Elsevier; 2005.
[57] Zou QH, Zhu CZ, Yang Y, et al. An improved approach to detection of amplitude of low-frequency fluctuation (ALFF) for resting-state fMRI: Fractional ALFF. J Neurosci Methods 2008;172:137–41.
[58] Wang JH, Zuo XN, Gohel S, et al. Graph theoretical analysis of functional brain networks: Test-retest evaluation on short- and long-term resting-state functional MRI data. PLoS One 2011;6:e21976.
[59] Yan CG, Wang XD, Zuo XN, et al. DPABI: Data processing & analysis for (resting-state) brain imaging. Neuroinformatics 2016;14:339–51.
[60] Wood SN. Generalized additive models: An introduction with R. 2nd ed. Chapman and Hall/CRC; 2017.
[61] Wickham H. ggplot2: Elegant graphics for data analysis. 2nd ed. Cham, Switzerland: Springer International Publishing; 2016.
[62] Venables WN, Ripley BD. Modern applied statistics with S. 4th ed. Springer; 2002.
[63] Cohen JE. Statistical power analysis for the behavioral sciences. Hillsdale, NJ: Lawrence Erlbaum Associates Inc.; 1988.
[64] Lillie EM, Urban JE, Lynch SK, et al. Evaluation of skull cortical thickness changes with age and sex from computed tomography scans. J Bone Miner Res 2016;31:299–307.
[65] Michel CM, Brunet D. EEG source imaging: A practical review of the analysis steps. Front Neurol 2019;10:325.
[66] Roche AF. Increase in cranial thickness during growth. Hum Biol 1953;25:81–92.
[67] Torimitsu S, Nishida Y, Takano T, et al. Differences in biomechanical properties and thickness among frontal and parietal bones in a Japanese sample. Forensic Sci Int 2015;252:e191–6.
[68] Mikkonen M, Laakso I, Tanaka S, et al. Cost of focality in tDCS: Interindividual variability in electric fields. Brain Stimul 2020;13:117–24.
[69] Arora Y, Chowdhury SR. Cortical excitability through anodal transcranial direct current stimulation: A computational approach. J Med Syst 2020;44:48.
[70] Kashyap R, Bhattacharjee S, Arumugam R, et al. Focality-oriented selection of current dose for transcranial direct current stimulation. J Pers Med 2021;11:940.
[71] Khan A, Antonakakis M, Vogenauer N, et al. Individually optimized multi-channel tdcs for targeting somatosensory cortex. Clin Neurophysiol 2022;134:9–26.
[72] Klaus J, Schutter D. Electrode montage-dependent intracranial variability in electric fields induced by cerebellar transcranial direct current stimulation. Sci Rep 2021;11:22183.
[73] Saturnino GB, Madsen KH, Siebner HR, et al. How to target inter-regional phase synchronization with dual-site transcranial alternating current stimulation. Neuroimage 2017;163:68–80.
[74] Saturnino GB, Siebner HR, Thielscher A, et al. Accessibility of cortical regions to focal tES: Dependence on spatial position, safety, and practical constraints. Neuroimage 2019;203:116183.

Weiwei Ma obtained her Master's degree in 2024 under the supervision of Prof. Yiheng Tu from the Institute of Psychology, Chinese Academy of Sciences. She received her B.E. degree from Shanghai Jiao Tong University. Her current research interest mainly focuses on individualized transcranial neuromodulation.

Yiheng Tu is a professor at the Institute of Psychology, Chinese Academy of Sciences. His laboratory investigates the neural representation and modulation of pain using brain imaging, computational modeling, and neural engineering techniques.